Designing LPG-OADM Based on a Finite Element Method and an Eigenmode Expansion Method

Yue Jing He and Xuan Yang Chen

***Abstract*—This study proposes a visual, graphical, and simplistic numerical simulation method for a long period fiber gratings optical add-drop multiplexer (LPG-OADM), as opposed to the well-known traditional mode-coupled theory. This method combines the finite element method and the eigenmode expansion method, where the finite element method is used to solve all existing guided modes. The eigenmode expansion method was used to calculate the energy transfer phenomenon of the guided modes in the LPG-OADM. This study provides a detailed explanation of the key reasons why the periodic structure of the LPG-OADM can achieve significantly superior results for our method compared to those obtained using other numerical methods, such as the finite-difference time-domain and beam propagation methods. All existing numerical simulation methods focus on large-sized periodic components; only the method established in this study has 3-D design and analysis capabilities. This study used actual examples to verify that, under the operating wavelength of $\lambda = 1550$ nm, the LPG-OADM designed using this method would have the full-width half-maximum of 0.2846 nm, and an insertion loss and homo-dyne crosstalk of nearly 0. That is, the LPG-OADM designed using this method can reach the ITU specification for the dense wavelength-division multiplexer bandwidth. The primary objective of this study is to use the combination of these two numerical simulation methods in conjunction with a rigorous, simple, and comprehensive design flow to provide a graphical and simplistic simulation technique that reduces the learning time and professional threshold requirements for the design and application of LPG-OADM.**

***Index Terms*—Optical add-drop multiplexer, eigenmode expansion method, finite element method, long-period fiber grating.**

I. Introduction

THE most critical component of developing a wavelength-division multiplexing system is the optical add-drop multiplexer (OADM). A simple OADM device that adds and/or drops a designed channel is a building block of the complicated optical fiber communication system. Over the past several decades, numerous types of OADMs have been proposed, such as the well-known structure that consists of a fiber Bragg grating and two optical circulators [1], [2], the Mach–Zehnder structure that relies on the interference between two lights that are reflected by Bragg gratings [3], [4], and the configuration based on a null coupler with a tilted grating in the waist [5]. In 2000, a simple architecture consisting of two parallel long-period fiber gratings was proposed by Chiang *et al.* [6]. This device is based on mode coupling by properly designing the period of long period fiber grating (LPG) and the power coupling between two parallel and identical optical fibers.

LPG that is written periodically by ultraviolet light into the core layer of a photosensitive optical fiber can couple the power among the copropagating modes. The coupling between the core mode HE_{11} and the cladding modes has been used extensively for band rejection filters, gain flatteners, and dispersion compensators [7]–[9]. For a given azimuthal number l, there are typically several hundred cladding modes at the near-infrared wavelength in a traditional communication fiber. According to the fundamental property of modes, the higher the order of the cladding mode, the farther the field can extend. A high-order cladding mode is more sensitive to the variations of the environment than is a low-order mode. Therefore, various sensors based on high-order cladding modes have been proposed in recent years [10]–[13]. In addition, LPG can function as an OADM component [14], [15], optical fiber surface plasmon resonance sensors [16], [17], and so on.

So far, traditional mode-coupled theory has been one of the most frequently used techniques in the research of LPG-OADM characteristics and related applications. For a scholar who has recently entered the LPG-OADM field, learning this theory is a critical and indispensable process in comprehending the physical concepts of the LPG-OADM. Traditional mode-coupled theory plays a pivotal role in understanding of the LPG-OADM related characteristics. Later are three brief descriptions that introduce how to employ traditional mode-coupled theory to conduct LPG-OADM analyses and design.

A. The Mathematical Modal of LPG

The general geometry structure of the optical fiber comprises three layers of media: a core layer, cladding layer, and surrounding layer. In addition, the related parameters of the various media layers are $a_1 = 2.25$ μm, $a_2 = 62.5$ μm, $n_1 = 1.45$, $n_2 = 1.43$, and $n_3 = 1$. A schematic diagram is shown in Fig. 1. The ideal radius of the surrounding layers should be infinite. After determining the geometric structure of the fiber cross section (*XY* plane), Maxwell equations are applied with boundary conditions to derive the dispersion relation equations. Finally, all guided modes that exist in the structure are obtained, and each guided mode has a corresponding effective refractive index of n_{eff} [18], [19]. Explained from a purely mathematical perspective, modes are solutions to differential equations that can satisfy specific boundary conditions. Unless

Manuscript received November 29, 2012; revised March 19, 2013; accepted April 1, 2013. Date of publication April 4, 2013; date of current version May 6, 2013. This work was supported by the National Science Council of Taiwan under Grant NSC 101-2622-E-167-007-CC3. The review of this paper was arranged by Associate Editor M. De Vittorio.

The authors are with the Department of Electronic Engineering, National Chin-Yi University of Technology, Taichung 41170, Taiwan (e-mail: yuejing@ncut.edu.tw; her.jing@msa.hinet.net).

Color versions of one or more of the figures in this paper are available online at http://ieeexplore.ieee.org.

Digital Object Identifier 10.1109/TNANO.2013.2256925

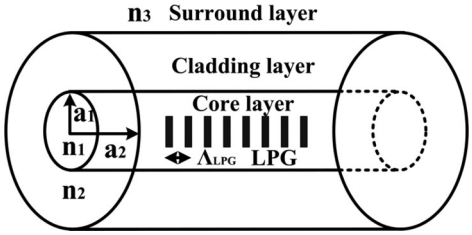

Fig. 1. A geometric and parameter diagram of a typical optical fiber and LPG.

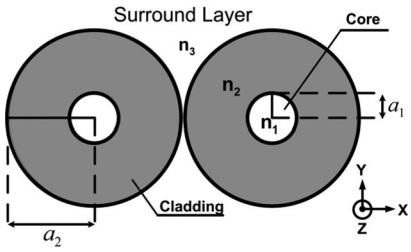

Fig. 2. Sectional view (*XY* plane) of the LPG-OADM.

otherwise specified, this study focused only on the analysis of single mode communication optical fibers with an operating wavelength of $\lambda = 1550$ nm. That is, we would obtain one core mode $n_{\text{eff}}^{\text{core}}(n_2 < n_{\text{eff}}^{\text{core}} < n_1)$ and nearly infinite cladding modes $n_{\text{eff}}^{\text{cladding}}$ $(n_3 < n_{\text{eff}}^{\text{cladding}} < n_2)$.

For LPG production, single mode optical fibers that used photosensitive materials in the core layer were first selected. Then, ultraviolet light was used to irradiate the amplitude mask with specific periods to enable the power to provide constructive and destructive interferences on the single-mode fiber and to further change the core layer refractive index. The mathematical model for uniform fiber grating is expressed as follows:

$$n_1(z) = n_1 + n_1\sigma\left[1 + \cos\left(\frac{2\pi}{\Lambda_{\text{LPG}}}z\right)\right] \tag{1}$$

where σ is the UV-induced refractive index variation, $n_1\sigma$ is the peak induced-index change, and Λ_{LPG} is the period of the LPG. From a mathematical perspective, before fiber grating occurred, all the modes in the fiber waveguides were orthogonal to each other. That is, during the entire transmission process, power between the modes could not be exchanged or coupled. However, after the LPG was written to the core layer, it generated a power perturbation effect between the modes. Appropriately designed LPG periods Λ_{LPG} can break the orthogonality of original modes and achieve a power coupling phenomenon.

B. Description of the Geometric Structure and Working Principle of the LPG-OADM

The geometric structure of the LPG-OADM of this study was formed by the parallel arrangement of two optical fibers with the same LPG_{OADM}. The sectional view (*XY* plane) and the side view (*XZ* plane) are shown in Figs. 2 and 3, respectively. After the multiwavelength optical signal entered the LPG-OADM from Fiber 1 through the input port, the perturbation effect of the LPG_{OADM} allowed that the core mode (HE_{11}) of the specific wavelength (λ_1) in Fiber 1 is coupled to the cladding mode.

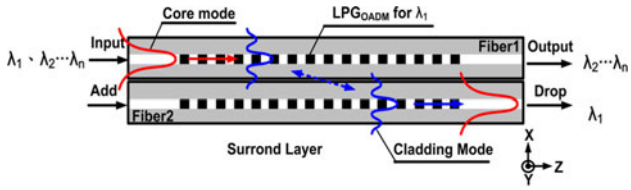

Fig. 3. Side view (*XZ* plane) of the LPG-OADM.

Next, the two nearby optical fibers acted like a 2×2 optical signal coupler to the cladding mode. Therefore, the cladding mode transmitted by Fiber 1 could be coupled to Fiber 2. Finally, because Fiber 2 used the same LPG_{OADM} as did Fiber 1, the cladding mode could be restored back into the original core mode. Based on the previous description, the process of combining all signal transmissions and mode conversions was actually the completion of the signal drop function of the LPG-OADM when viewed from a different angle. A schematic diagram is shown in Fig. 3. Because of the symmetric structure of LPG-OADM, if the optical signal was inputted through the added port of Fiber 2, this signal was eventually outputted from the output port of Fiber 1. This achieved the add function of LPG-OADM. All of the wavelengths for multiwavelength optical signals that were unaffected by LPG_{OADM} completely entered through the input port and were outputted through the output port.

Based on the previous description, it is apparent that the cladding mode must be able to be coupled from Fibers 1 to 2, acting like a 2×2 optical signal coupler. When the distance between two optical fibers increases, the ability to traverse the 2×2 optical signal coupler decreases for a given cladding mode. Therefore, for the LPG-OADM to enable power output at the Drop or Add ports, the completed LPG-OADM design must be longer. In this study, the LPG-OADM is designed by shortening the distance between the two optical fibers (i.e., no space is left between the two parallel optical fibers) to optimize the performance of the 2×2 optical signal coupler. In practical fabrication, it is much more difficult to maintain a constant distance between two tiny optical fibers than to arrange two optical fibers in parallel adjacency. From the perspective of the mode, an increase in the order of the cladding mode is correlated with the greater extensibility of the power field on the cladding layer. Therefore, regarding the traversal ability of a 2×2 optical signal coupler, it is feasible to design the LPG-OADM with a high-order cladding mode. However, for LPG coupling mechanisms, the coupling ability between the core mode and the high-order cladding mode is relatively poor. Thus, to ensure the coupling of the core mode to the high-order cladding mode, a longer LPG is required. In summary, when the distance between the two optical fibers is increased, the use of the high-order cladding mode may not necessarily be a good solution for LPG-OADM design. Therefore, employing two optical fibers in parallel adjacency may be an optimal and simple solution for the LPG-OADM design, both in theoretical and practical terms.

Under the assumption that only four modes couplings can occur simultaneously, and according to the derivation of mode-coupled theory, the functions performed by the LPG-OADM

shown in Fig. 3 can be described by the following four mathematical equations [14]:

$$A'_{co-1}(z) = ik_{co-1,cl-1}A_{cl-1}(z)\exp(-i\delta z) \quad (2)$$

$$A'_{cl-1}(z) = ik_{co-1,cl-1}A_{co-1}(z)\exp(i\delta z) + ic_{cl-1,cl-2}A_{cl-2}(z) \quad (3)$$

$$A'_{cl-2}(z) = ik_{co-2,cl-2}A_{co-2}(z)\exp(i\delta z) + ic_{cl-1,cl-2}A_{cl-1}(z) \quad (4)$$

$$A'_{co-2}(z) = ik_{co-2,cl-2}A_{cl-2}(z)\exp(-i\delta z) \quad (5)$$

with

$$\delta = \beta_{co-1} - \beta_{cl-1} + \sigma_{co-1,co-1} - \sigma_{cl-1,cl-1} - c_{cl-1,cl-1} - (2\pi/\Lambda_{\mathrm{OADM}}) \quad (6)$$

$$k_{co-1,cl-1} = \frac{\omega\varepsilon_0 n_1^2\sigma}{2}\int_0^{2\pi}\int_0^{a_1} r(E_r^{co-1}E_r^{cl-1} + E_\varphi^{co-1}E_\varphi^{cl-1} - E_z^{co-1}E_z^{cl-1})drd\varphi \quad (7)$$

$$k_{co-2,cl-2} = k_{co-1,cl-1} \quad (8)$$

$$\sigma_{co-1,co-1} = \frac{\omega\varepsilon_0 n_1^2\sigma}{2}\int_0^{2\pi}\int_0^{a_1} r(E_r^{co-1}E_r^{co-1} + E_\varphi^{co-1}E_\varphi^{co-1} - E_z^{co-1}E_z^{co-1})drd\varphi \quad (9)$$

$$\sigma_{cl-1,cl-1} = \frac{\omega\varepsilon_0 n_1^2\sigma}{2}\int_0^{2\pi}\int_0^{a_1} r(E_r^{cl-1}E_r^{cl-1} + E_\varphi^{cl-1}E_\varphi^{cl-1} - E_z^{cl-1}E_z^{cl-1})drd\varphi \quad (10)$$

$$c_{cl-1,cl-2} = \frac{\omega\varepsilon_2}{2}\int_0^{2\pi}d\varphi\int_0^{a_1} r(E_r^{cl-1}E_r^{cl-2} + E_\varphi^{cl-1}E_\varphi^{cl-2} - E_z^{cl-1}E_z^{cl-2})dr \quad (11)$$

$$c_{cl-1,cl-1} = \frac{\omega\varepsilon_2}{2}\int_0^{2\pi}d\varphi\int_0^{a_1} r(E_r^{cl-1}E_r^{cl-1} + E_\varphi^{cl-1}E_\varphi^{cl-1} - E_z^{cl-1}E_z^{cl-1})dr \quad (12)$$

where $A_{co-1}(z)$ is the amplitude of core mode HE_{11} propagating in Fiber 1, $A_{cl-1}(z)$ is the amplitude of cladding mode ν propagating in Fiber 1, $A_{co-2}(z)$ is the amplitude of core mode HE_{11} propagating in Fiber 2, $A_{cl-2}(z)$ is the amplitude of cladding mode ν propagating in Fiber 2, $k_{co-1,cl-1}$ is the "ac" coupling coefficient between core mode HE_{11} and cladding mode ν for Fiber 1, $k_{co-2,cl-2}$ is the "ac" coupling coefficient between core mode HE_{11} and cladding mode ν for Fiber 2, $\sigma_{co-1,co-1}$is the "dc" coupling coefficient of core mode HE_{11} for Fiber 1, $\sigma_{cl-1,cl-1}$ is the "dc" coupling coefficient of cladding mode ν for Fiber 1, $c_{cl-1,cl-2}$ is the cross coupling coefficient between Fibers 1 and 2 for cladding mode ν, $c_{cl-1,cl-1}$ is the self-coupling coefficient of cladding mode ν for Fiber 1, σ is the UV-induced refractive index variation, and ε_2 is the dielectric constant of Fiber 2. The period and length of the $\mathrm{LPG}_{\mathrm{OADM}}$ required for the optimal design of this element can be obtained based on the derivation processes in [14], which are shown as follows:

$$\Lambda_{\mathrm{OADM}} = \frac{2\pi}{\beta_{co-1} - \beta_{co-1} + k_{co-1,co-1} - k_{cl-1,cl-1} - c_{cl-1,cl-1}} \quad (13)$$

$$L_{\mathrm{OADM}} = \frac{\sqrt{3}\pi}{2k_{co-1,cl-1}}. \quad (14)$$

C. Definition of Bar and Cross Transmission Power for Spectrum

To analyze the spectral characteristics of the LPG-OADM, the bar transmission power and cross transmission power were defined using the following mathematical equations:

$$t = \frac{|R(z)|^2}{|R(0)|^2} \quad (15)$$

$$t_\times = \frac{|S(z)|^2}{|R(0)|^2}. \quad (16)$$

where $R(z)$ represents the magnitude of the field for the core mode and $S(z)$ represents the magnitude of the field for the cladding mode. A power spectrum diagram of LPG-OADM can be obtained by drawing a diagram of the relationship between these two parameters and the wavelength. Simply put, the bar transmission power is the self-power ratio of the incident mode HE_{11} after traveling a certain distance (z) and when incidence occurs ($z = 0$). In other words, for incident mode HE_{11}, after traveling a certain distance z, if the power can be coupled to other modes, the power ratio of the modes and the incidence ($z = 0$) of HE_{11} denote the cross transmission power.

The preceding introduction endeavored to analyze and simplify the four-modes coupled-mode theory and provided a comprehensive introduction to its physical concepts in layman's terms, using as few mathematical equations as possible. Traditional four-modes coupled-mode theory is not only a significant mathematical burden for novice learners of LPG-OADM, but its daunting difficulty is dreaded among application-level designers. Obviously, for novice learners and application-level designers of LPG-OADM, the completion of LPG-OADM design and analysis would invariably involve considering numerous mathematical equations, which indirectly raises the requirements and prerequisite domain knowledge for entering this field. In this study, a numerical technique was employed that combines the finite element method (FEM) and eigenmode expansion method (EEM) in the LPG-OADM design and simulation. The study demonstrates that by using this numerical technique, the design and analysis of LPG-OADM can be effortlessly accomplished without using any mathematical equations by novice learners and application-level designers.

In addition, the extensive use of graphics may help novice learners and application-level designers gain a visualized understanding of the transmission of optical signals in LPG-OADM that is otherwise unachievable through the traditional four-modes coupled-mode theory. This constitutes the contribution and novelty of this study. To the best knowledge of the author, the significance and original findings reported in this study are

not published elsewhere. The traditional coupled-mode theory uses the perturbation theory, allowing the input mode to interact with other guided modes during transmission to achieve power exchange. As a well-established theory, the traditional coupled-mode theory has been extensively applied in various domains. Power conversion among various modes is the core concept of the traditional coupled-mode theory. However, such a core value cannot be graphically manifested. By contrast, this study represents the process of power conversion in graphical form, thus offering originality and contributions to this literature.

A crucial blind spot exists in the literature pertaining to the traditional coupled-mode theory. Specifically, the "ac" coupling coefficient is a key parameter for the entire traditional coupled-mode theory; in addition, it is a key element for power coupling, without which no power coupling could be generated between different modes. Among numerous published works in which the traditional coupled-mode theory is applied, few have literally provided the calculation result of the "ac" coupling coefficient. The failure to provide a calculation result causes their research to be proven entirely erroneous. Conversely, this further highlights the value and significance of this study. Using the proposed numerical method, novice learners and application-level designers may directly observe the transmission of optical signals in the LPG-OADM from the calculation results, which helps explain the generation of coupling effects through LPG-OADM. In summary, the core contribution of this study is in its simplicity and graphical representation.

The remaining content in this study is as follows. Section II provides a brief introduction to theories related to the FEM. Regarding numerical methods, the decomposition resolution of triangular elements critically affects the correctness of the modes obtained. From a mathematical perspective, if all the modes that are obtained are correct, the orthogonal values between the modes must be 0. Therefore, this study used a reverse-thinking method by initially determining an acceptable orthogonal value (10^{-4}, –4 dB), and then adjusting the decomposition resolution for simulation. In addition, the modes obtained at any time were inspected to determine whether they conformed to the relevant norm specifying orthogonal values of less than 10^{-4} (–4 dB). Section III introduces theories related to the EEM and provides a detailed explanation of how the EEM allows guided modes to conduct transmissions in LPG-OADM structures. In addition, this section specifies the chief reason why this method is significantly superior to the finite-difference time-domain (FDTD) method and the beam propagation method. However, this numerical method exhibits accuracy problems. The Fourier series expansion is the primary principle that enables light wave transmissions to be performed using this numerical method. That is, if the number of guided modes is insufficient during the transfer process, even in nonabsorbent media, the total power is gradually reduced as the transmission distance increases. This study used the reverse-thinking method to utilize various numbers of guided modes to perform transmissions, consider the power dissipation, and determine the number of guided modes for this study. A relationship diagram was used sporadically to verify power loss and distance during the design process.

In Section IV, the contents of Sections II and III are summarized to propose a rigorous, simplistic, and comprehensive design process for analyzing and designing the LPG-OADM. This section presents numerous graphical simulation results to visually and simplistically supplement the formulaic and abstract content of traditional form of mode-coupled theory learning. In the final section, the numerical simulation methods proposed in this study are summarized and all the data obtained in Section IV are collated to verify that the method proposed in this study does provide a visual and simplistic simulation technique for large-scale periodic components and reduces the learning time and professional threshold required for designing and applying the LPG-OADM.

II. The FEM

The FEM is a numerical simulation method that has been widely used in various fields of engineering. Because the principles of the algorithm used in this method have been thoroughly explained in numerous studies [20], in this section, we only briefly introduce the main concepts of this method. Instead, we focused on how the FEM can be used to solve all existing guided modes in a fiber structure.

The FEM is a numerical method used to solve partial differential equations (PDEs) that satisfy boundary conditions. This method is based on the variational principle, domain decomposition, and interpolation function. The FEM uses the variation principle (the variation algorithm) to transform the original problem (PDE with boundary conditions) into functional extreme value problems different from the original problem but with equivalent values. In other words, the same physical problem has two mathematical descriptions. That is, "boundary conditions + PDE = the functional for determining the minimum value." After determining the functional extreme value problem equivalent to the original problem, we applied the interpolation function and decomposed the domain we hoped to solve to convert the problem in which the functional solved for the minimum value into a set of multiple linear algebraic equations. We obtained the solution to the original problem by solving these linear algebraic equations. The algorithm of the FEM comprises the following five steps.

1) Use the equivalent functional for solving the minimum value problem to replace the PDE with boundary conditions.
2) Divide the geometric domain to be solved into several sufficiently small segments. These segments are known as elements, such as triangular or quadrilateral elements. The objects connecting elements are nodes, and the unknown variables of the nodes are the desired answers.
3) The actual unknown function in each element is approximated by an appropriate interpolation function. The easiest interpolation function to perform is the linear interpolation function. Thus, the polynomial functions formed by nodes can be employed for the approximation of the true function to be solved in each element. This polynomial coefficient is the shape function.
4) Substitute this polynomial function into the functional to calculate a minimum value and obtain a set of simultaneous equations.

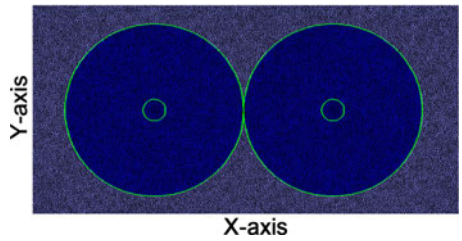

Fig. 4. A triangular element decomposition schematic diagram for the cross sectional (*XY*) plane of the LPG-OADM.

5) Enter the boundary conditions into the simultaneous equations, and solve these equations using the Gaussian elimination method. Thus, the answer to all nodes in the domain to be solved can be obtained. After the answer to each node is obtained, each true function to be solved within the element can be further approximated using the polynomial function of the node. All unknown variables or values in the entire geometric domain to be solved can be obtained.

In this study, the triangular element method was used to decompose the geometric domain of the cross section (*XY* plane) of the LPG-OADM. The schematic diagram is shown in Fig. 4. The diagram clearly shows that the higher the decomposition resolution, the more accurate the calculation results, and the relative number of calculations increases significantly. Therefore, achieving appropriate domain discretization becomes a core technique in the FEM. As mentioned, from a mathematical perspective, all theoretical modes must be mutually orthogonal. The orthogonal value can be determined using the following equation:

$$\int_{A\infty} E_{t\nu} \times H_{t\mu} \bullet \hat{z}\, dA = \int_{A\infty} E_{t\mu} \times H_{t\nu} \bullet \hat{z}\, dA = 0 \text{ for } \upsilon \neq \mu. \tag{17}$$

However, numerical simulations invariably generate problems of excessive memory capacity and time requirements for mode solutions. This study, to coordinate with the server's calculation capabilities, examined the orthogonal values of the obtained modes to appropriately adjust the decomposition resolutions of the triangles. Unless otherwise noted, this study used an orthogonal value of less than 10^{-4} (-4 dB) as a guideline for all decomposition resolutions. In order to satisfy this guideline, the minimum number of the elements in the core layer is $\sim$100, and the minimum number of the elements in the cladding layer is $\sim$1800. All guided modes within the structure could be solved after completing the decomposition process, where the operating wavelength was $\lambda = 1550$ nm. Because a single mode fiber was used, only one core mode was obtained, that is, HE_{11}, with an effective refractive index of $n_{\text{eff}}^{\text{core}}$ $(n_2 < n_{\text{eff}}^{\text{core}} < n_1)$ and an approximately infinite number of cladding modes with the effective refractive index $n_{\text{eff}}^{\text{cladding}}$ $(n_3 < n_{\text{eff}}^{\text{cladding}} < n_2)$.

The cross-sectional plane of the LPG or LPG_{OADM} previously described was uniform. Therefore, when the core mode (HE_{11}) entered the LPG or LPG_{OADM} domain, the mode-coupling phenomenon only occurred between HE_{11} and the cladding modes of the azimuthal order $l = 1$. Therefore, this study focused solely on solving and exploring $l = 1$ cladding modes. The FEM can be used to obtain core mode HE_{11} and its 2-D and 3-D power distribution diagrams, as shown in Fig. 5(a) and (b), where its effective refractive index is $n_{\text{eff}}^{\text{core}} = 1.43944$. For cladding mode $\nu = 1$, its 2-D and 3-D power distribution are shown in Fig. 5(c) and (d), and its effective refractive index

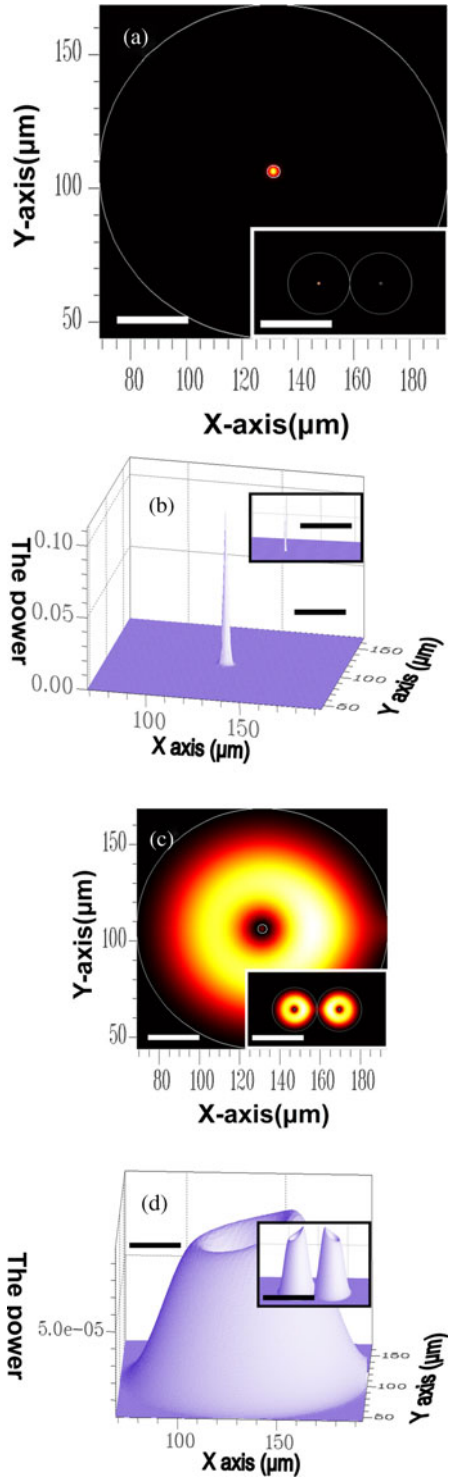

Fig. 5. (a) The 2-D power distribution of the core mode. (b) The 3-D power distribution of the core mode. (c) The 2-D power distribution of the cladding mode ($\nu = 1$). (d) The 3-D power distribution of the cladding mode ($\upsilon = 1$) with scale bar 25 and 120 μm on the inset.

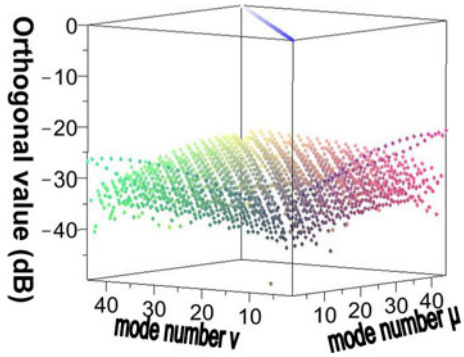

Fig. 6. The relationships between the orthogonal values of the 44 modes for Fiber 1.

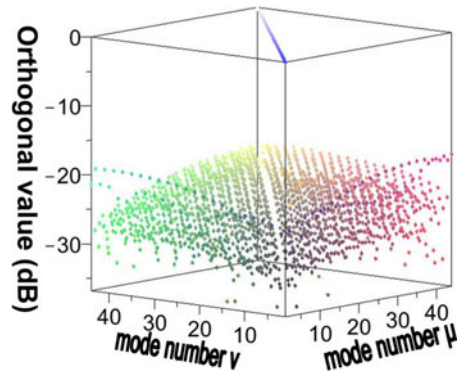

Fig. 7. The relationships between the orthogonal values of the 44 modes for LPG-OADM.

was $n_{\text{eff}}^{\nu=1} = 1.429951$. A total of 44 guided modes, including one core mode (HE_{11}) and 43 cladding modes ($\nu = 1 - 19$; $l = 1$), were solved during the preliminary process. In addition, orthogonal values among the 44 modes for Fiber 1 and LPG-OADM were calculated and examined, and the results are shown in Figs. 6 and 7. Clearly, in addition to each mode having a self-orthogonal value of 1 (0 dB), the orthogonal values between two different modes could satisfy the requirement of being less than 10^{-4} (-4 dB).

III. The EEM

The chief reason for employing this method was to allow the guided modes to conduct power transfers in an optical fiber structure. First, this method captured one segment object from the LPG-OADM periodic object and the length of the segment object is one period of the LPG-OADM periodic object, as shown in Fig. 8. The diagram clearly indicates that the LPG-OADM periodic object is composed of N segment objects. The length of each segment object represents one LPG period, as well as that of the LPG-OADM periodic object. Further cutting of each segment object produces miniobjects called block objects (Bk) with a length of dΛ. Each block object is considered a uniform LPG-OADM waveguide possessing a fixed refractive index value in the core layer. The contact surface between block object k–1 (Bk_{k-1}) and block object k (Bk_k) is called junction k–1 (J_{k-1}), which is presented in Segment (1) of Figs. 8 and 9.

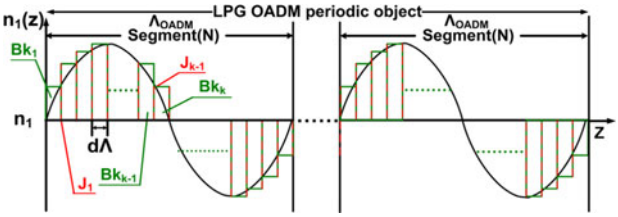

Fig. 8. Each cut block object in a segment object is considered a uniform waveguide with a fixed refractive index.

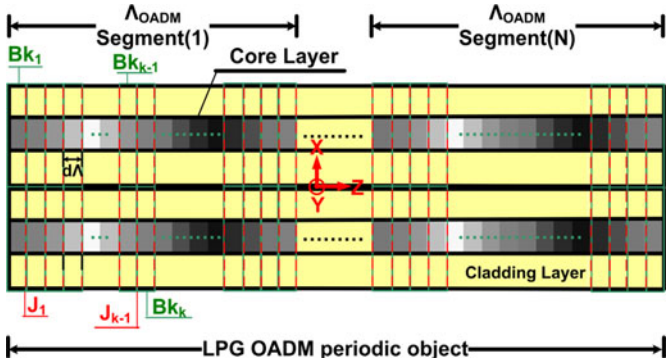

Fig. 9. Cutting schematic for the LPG-OADM periodic object.

The diagram clearly shows that by employing the same cutting mechanism, the block objects obtained from cutting segment object (m) and segment object (n) are identical completely. In other words, under the same cutting procedure, completing the cutting computation for a segment object equates to completing the cutting computation for an entire LPG-OADM periodic object. In this study, we cut a segment object into 300 uniform block objects. The EEM targeted one segment object from the LPG-OADM periodic object and the segment was cut into 300 uniform block objects. In each block object, the guided modes that may exist were recalculated. Next, power conversions between block objects were performed using the Fourier series expansion method. The steps in this procedure can also be performed to complete the power transfers of the entire LPG-OADM [21]–[23].

This simple description clearly indicates that, for periodic elements, the guided modes of each period are the same. Therefore, using the finite method to solve the guided modes, this study only needed to complete calculations for a certain period, as shown in Fig. 8. This significantly reduced the calculation time and memory capacity required to complete the entire element simulation. Therefore, the combination of the FEM and the mode expansion method is extremely appropriate for designing elements with periodic structures, such as LPG-OADMs, long-period fiber-grating surface-plasmon-resonance sensors, D-type long-period fiber-grating surface-plasmon-resonance sensors, and crystal D-type long-period fiber-grating surface-plasmon-resonance sensors. Currently, using the calculation mechanisms of the FDTD method, under an operating wavelength of $\lambda = 1550$ nm, an LPG-OADM with a length of 1 cm is colossal and cannot be simulated. Even using a supercomputer, calculations for 1 cm LPG-OADM require incredible amounts of

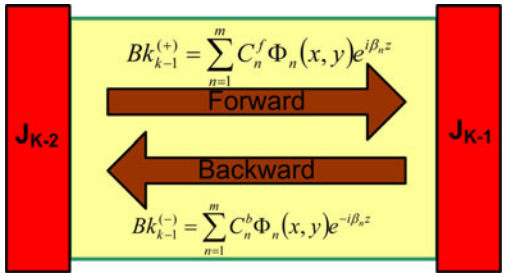

Fig. 10. Fourier series expansion for the forward and backward propagation modes.

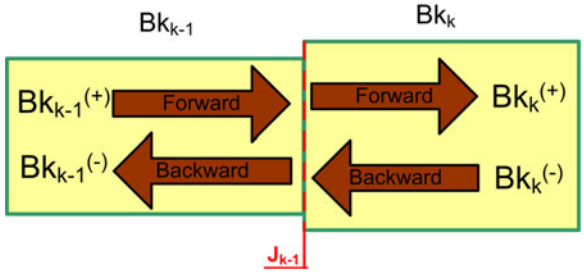

Fig. 11. The relationship between the field strength of the two adjacent uniform block objects Bk_{k-1} and Bk_k.

memory and computation time. Furthermore, calculations using the beam propagation method still possess excessive restrictions and errors for multiple reflective 3-D fiber-grating structures. The preceding descriptions clearly show that the single-period calculation characteristic is the primary reason that the combination of the FEM and the EEM is superior to the FDTD method and the beam propagation method.

Next, this study explains how the EEM is used for the power transmission of LPG-OADM. Based on the preceding descriptions, for one period, the LPG-OADM is decomposed into several uniform waveguides. For each uniform waveguide, it can be assumed that the solution to Maxwell's equations is (18), where the mode content Φ_n and the propagation constant β_n are the eigenfunction and the eigenvalue obtained using the FEM, respectively

$$E(x,y,z) = \Phi_n(x,y)e^{i\beta_n z}. \tag{18}$$

By combining (18) with the Fourier series expansion concept, and adding the entire forward propagation mode $Bk_k^{(+)}$, as shown in (19), and the back propagation mode $Bk_k^{(-)}$, as shown in (20), obtained using the FEM, where $m = 44$ was the guided mode amount, and C_n^f and C_n^b were the coefficients for each forward and backward mode field, as shown in Fig. 10, the electric and magnetic fields within the uniform block object Bk_{k-1} can be obtained, as shown in (21) and (22)

$$Bk_k^{(+)} = \sum_{n=1}^{m} C_n^f \Phi_n(x,y)\, e^{i\beta_n z} \tag{19}$$

$$Bk_k^{(-)} = \sum_{n=1}^{m} C_n^b \Phi_n(x,y)\, e^{-i\beta_n z} \tag{20}$$

$$E(x,y,z) = \sum_{n=1}^{m} (C_n^f e^{i\beta_n z} + C_n^b e^{-i\beta_n z}) E_n(x,y) \tag{21}$$

$$H(x,y,z) = \sum_{n=1}^{m} (C_n^f e^{i\beta_n z} - C_n^b e^{-i\beta_n z}) H_n(x,y). \tag{22}$$

After the propagated electromagnetic fields for a uniform block object Bk_{k-1} are obtained, power must be precisely transferred from Block object Bk_{k-1} to Block object Bk_k. Here, we used the scattering matrix to transform the forward and backward power propagation of two adjacent block objects, as shown in (23). In Fig. 11, $Bk_{k-1}^{(+)}, Bk_k^{(+)}$ and $Bk_{k-1}^{(-)}, Bk_k^{(-)}$ were the total of the forward and backward propagation modes for the uniform block object Bk_{k-1} and the uniform block object Bk_k, and J_{k-1} was the scattering matrix of the adjacent block object junctions

$$\begin{bmatrix} Bk_{k-1}^{(-)} \\ Bk_k^{(+)} \end{bmatrix} = J_{k-1} \begin{bmatrix} Bk_{k-1}^{(+)} \\ Bk_k^{(-)} \end{bmatrix}. \tag{23}$$

To convert power between adjacent block objects, we employed the Fourier series expansion to obtain the unknown junction scattering matrix J_{k-1}. Finally, the coupling effects of LPG-OADM could be accurately conducted and completed by following the steps of this method. After considering detailed descriptions of the EEM, we can clearly determine that for periodic objects, only one segment object (that is, one period) is required during the cutting and mode-solving procedures.

Then, by calculating each junction scattering matrix J_{k-1}, we can complete the simulation of the period object's modal transfer phenomenon. In summary, the ability to cut one single segment object and solve modes is the primary reason the EEM is superior to FDTD on calculation time and amount of memory used. In the traditional coupled-mode theory, the solution calculation of the guided modes occurred only at the beginning of the *XY* cross section, and throughout the entire process of the optical signal passing through the LPG-OADM, the guided modes were never recalculated. Therefore, the traditional mode-coupled theory emphasizes that the peak-induced index change ($\delta n = n_1 \sigma$) of the $\mathrm{LPG_{OADM}}$ cannot be excessive and must generally be smaller than 10^{-3}. Otherwise, mode-coupled theory exhibits significant errors. Compared to the traditional coupled-mode theory, the EEM employed in this study can detail cut one segment into 300 uniform block objects and resolve for the guided modes of each uniform block object. In other words, this method is not disadvantaged by requiring that the induced refractive index charge is not excessive. In addition, unless otherwise specified, all the induced refractive index changes in this study used $\delta n = n_1 \sigma = 1 \times 10^{-3}$ as the guideline.

According to the detailed description of the EEM, we observed that, in (19)–(22), m represents the number of guided modes and can critically affect the accuracy of the method. From a mathematical perspective, the Fourier series expansion must include all the guided modes that exist in the structure. However, this is impossible for numerical simulations because the time and memory required to perform such calculations are

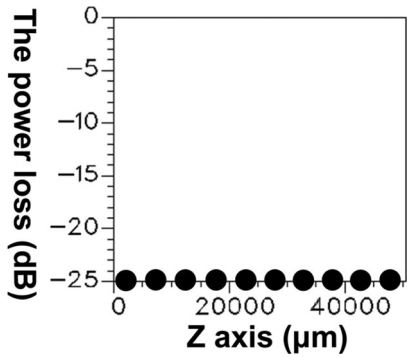

Fig. 12. The relationships between transmission distance and power dissipation for the eigenmode expansion method that employed 44 guided modes for Fiber 1.

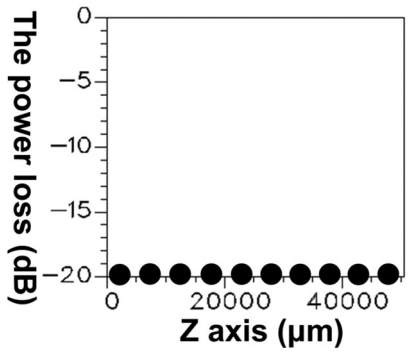

Fig. 13. The relationships between transmission distance and power dissipation for the eigenmode expansion method that employed 44 guided modes for LPG-OADM.

excessive and cannot bear the load. However, if the number of guided modes is insufficient, some power dissipation occurs during each pass through the scattering matrix for the adjacent block object junction. Therefore, this study used the reverse-thinking method and searched for the smallest m value that satisfied the requirement that the power dissipation value not exceed 10^{-4} (-4 dB). Figs. 12 and 13 show the relationships between the transmission distance and power dissipation of each Fourier series expansion when the 44 guided modes were utilized in the EEM ($m = 44$) for Fiber 1 and LPG-OADM, respectively. In this study, a segment object was uniformly cut into 300 uniform block objects. Using 300 uniform block objects and 44 guided modes, the results in Figs. 12 and 13 verify that the power loss of the EEM fully satisfied the $<10^{-4}$ (-4 dB) criterion. Therefore, unless otherwise specified, the standard number of all guided modes and block objects used in this study were 44 and 300, respectively.

IV. Design and Analysis of the LPG-OADM

Based on the numerical simulation methods described in Sections II and III, this section developed a rigorous, simplistic, and comprehensive design process (as shown in Fig. 14) that was used to complete the analysis and design of the LPG-OADM. The geometric structure of the LPG-OADM used for simulations in this section is shown in Fig. 15, where L_1 = 100 μm and L_3 = 100 μm were single-mode fibers, and

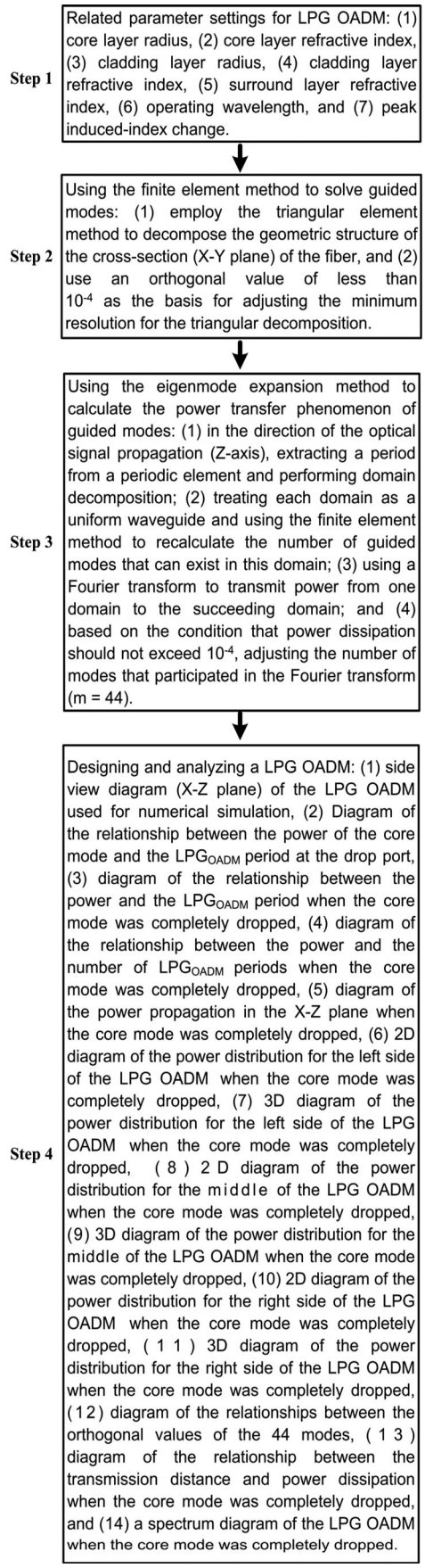

Fig. 14. Flowchart of the LPG-OADM design and analysis.

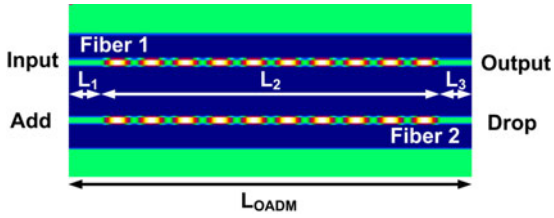

Fig. 15. Side view diagram (*XZ* plane) of the LPG-OADM used for numerical simulation.

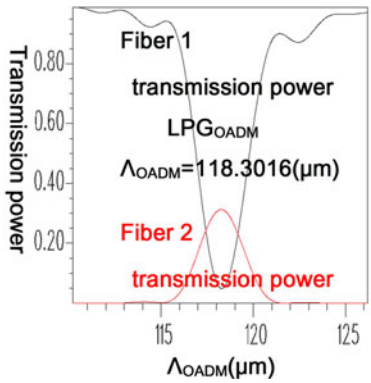

Fig. 16. Diagram of the relationship between the power of the core mode and the $\mathrm{LPG}_{\mathrm{OADM}}$ period at the drop port.

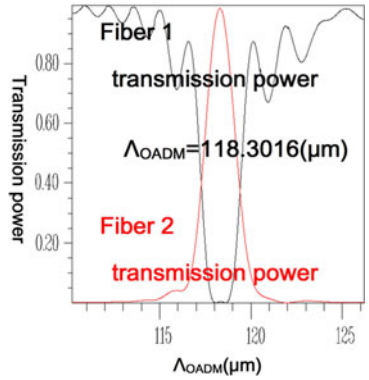

Fig. 17. Diagram of the relationship between the power and the $\mathrm{LPG}_{\mathrm{OADM}}$ period when the core mode was completely dropped.

$L_2 = \mathrm{N}_{\mathrm{OADM}} \times \Lambda_{\mathrm{OADM}}(\mu\mathrm{m})$ was the single-mode fiber of $\mathrm{LPG}_{\mathrm{OADM}}$. In addition, the distance between the two fibers was 0, the operating wavelength was $\lambda = 1550$ nm, and the related parameters of the various media layers are $a_1 = 2.25$ μm, $a_2 = 18$ μm, $n_1 = 1.45$, $n_2 = 1.43$, and $n_3 = 1.425$.

Combining the FEM and the EEM enabled the rapid scanning of the diagram of the relationship between the power of the core mode and the $\mathrm{LPG}_{\mathrm{OADM}}$ period at the drop port, as shown in Fig. 16. The information in this figure shows the period of $\mathrm{LPG}_{\mathrm{OADM}}$ required to design the completely dropped core mode. Fig. 17 shows a diagram that illustrates the relationship between power and the $\mathrm{LPG}_{\mathrm{OADM}}$ period when the core mode was completely dropped. Fig. 18 shows a diagram of the relationship between power and the number of $\mathrm{LPG}_{\mathrm{OADM}}$ periods when the core mode was completely dropped. Combining Figs. 17 and 18, it is easy to determine that, during the Λ_{OADM}

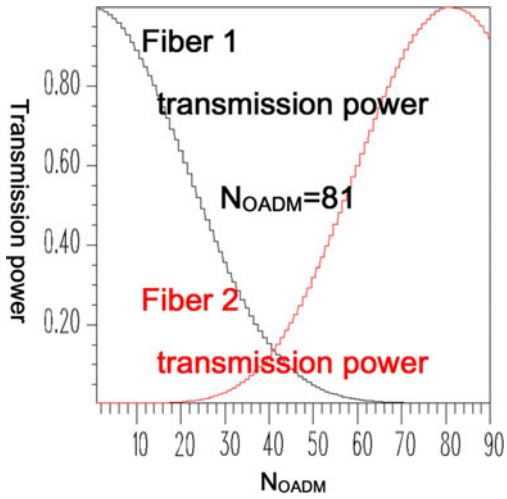

Fig. 18. Diagram of the relationship between the power and the number of $\mathrm{LPG}_{\mathrm{OADM}}$ periods when the core mode was completely dropped.

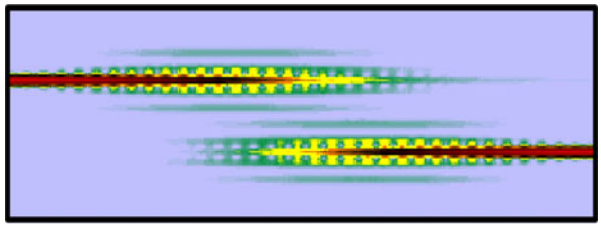

Fig. 19. Diagram of the power propagation in the *XZ* plane when the core mode was completely dropped.

$= 118.3016$ μm $\mathrm{LPG}_{\mathrm{OADM}}$ period and when the number of the $\mathrm{LPG}_{\mathrm{OADM}}$ period was 81, the LPG-OADM reached a condition where power was almost completely dropped. Based on these two parameters, this study inputted the core mode (HE_{11}) from the input port of Fig. 15 to observe the power transmission condition of HE_{11} at the $Y = 0$ plane or the *XZ* plane. The results are shown in Fig. 19. The inputted power had reached an almost dropped phenomenon. In addition, to verify the accuracy of the power drop, the 2-D and 3-D power distribution diagrams were intercepted from the left, middle, and right sides of Fig. 19, respectively. The results shown in Figs. 20–22 verified the correctness of the methods proposed in this study. To comply with the design process norm of Step 2, the orthogonal values of this sample were calculated and verified, and the results are shown in Fig. 23. In addition to having a self-orthogonal value of 1 (0 dB) for each mode, the orthogonal values between two different modes can satisfy the requirements of being less than 10^{-4} (-4 dB). In addition, the transmission distance and power dissipation conditions of this example must be examined. As shown in Fig. 24, the power dissipation can satisfy the less than 10^{-4} (-4 dB) requirement specified in Step 3 of the design process.

Finally, the spectrum of LPG-OADM was calculated using the obtained parameter of $\Lambda_{\mathrm{OADM}} = 118.3016$ μm and the number of periods $\mathrm{N}_{\mathrm{OADM}} = 81$. To verify that at the operating wavelength ($\lambda = 1550$ nm) the LPG-OADM designed in this study has an insertion loss and homo-dyne crosstalk approximating 0,

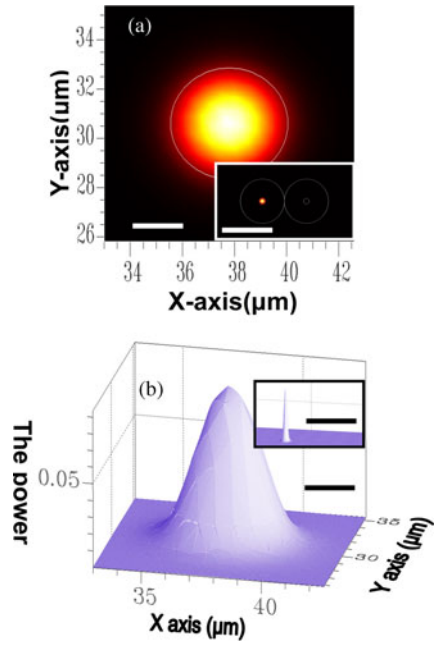

Fig. 20. The power distribution at input port of LPG-OADM when the design of LPG-OADM was completed. (a) A 2-D diagram. (b) A 3-D diagram with scale bar 2 and 50 μm on the inset.

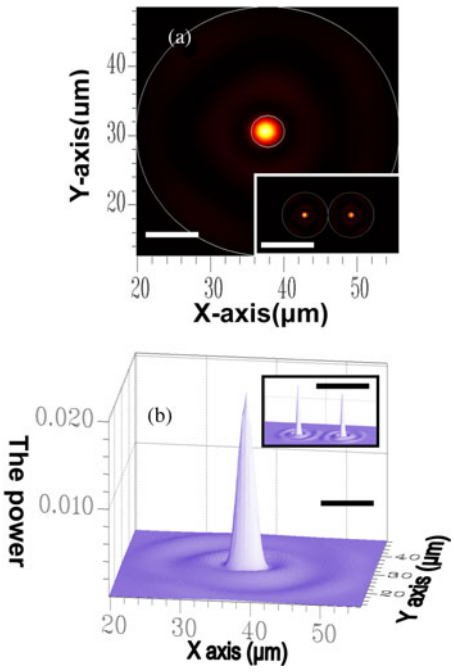

Fig. 21. The power distribution at middle of LPG-OADM when the design of LPG-OADM was completed. (a) A 2-D diagram. (b) A 3-D diagram with scale bar 7 and 50 μm on the inset.

the diagrams of the LPG-OADM spectrum were plotted in the decibel scale as shown in Fig. 25 which clearly demonstrates the required verification. Because the full-width half-maximum (FWHM) bandwidth of the designed LPG-OADM cannot be clearly seen from the spectrum diagram in the decibel scale, a closeup of the transmission power between 0 and -3 dB was extracted from Fig. 25, as shown in Fig. 26. From this closeup

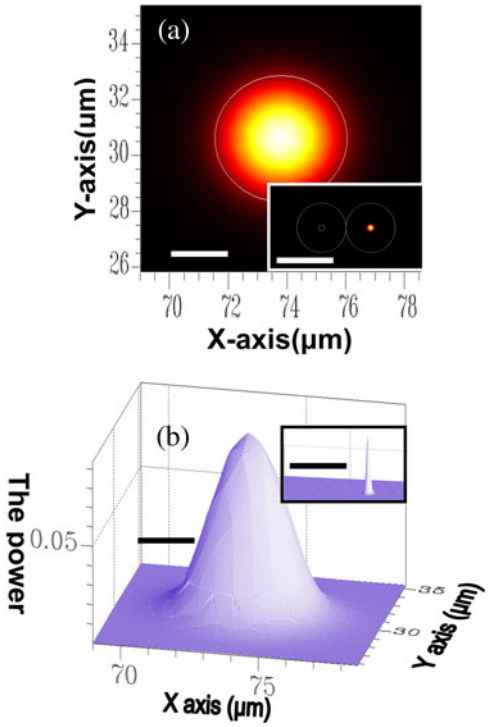

Fig. 22. The power distribution at drop port of LPG-OADM when the design of LPG-OADM was completed. (a) A 2-D diagram. (b) A 3-D diagram with scale bar 2 and 50 μm on the inset.

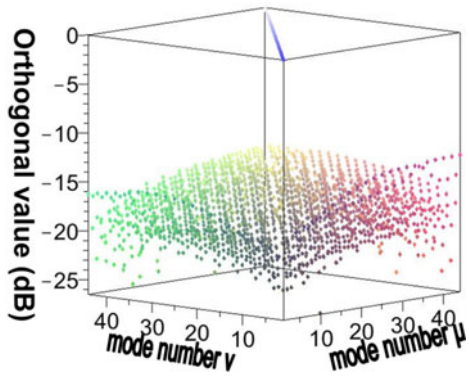

Fig. 23. Diagram of the relationships among the orthogonal values of the 44 modes when the core mode was completely dropped.

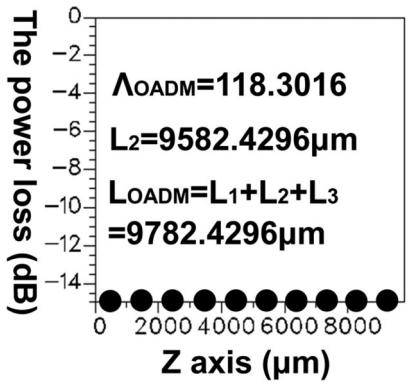

Fig. 24. Diagram of the relationship between the transmission distance and power dissipation when the core mode was completely dropped.

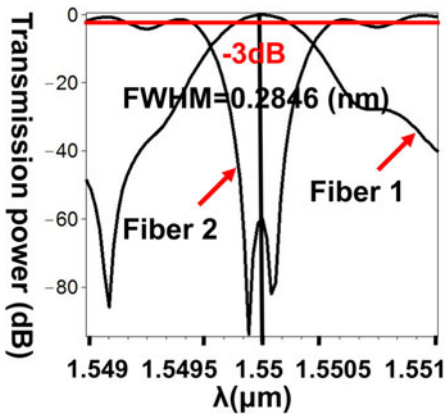

Fig. 25. A spectrum diagram of the LPG-OADM when the core mode was completely dropped.

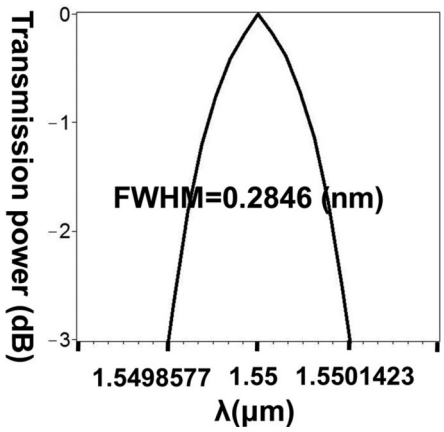

Fig. 26. A spectrum diagram of the LPG-OADM for the –3 dB bandwidth (FWHM).

figure, the LPG-OADM designed in this study clearly possesses an FWHM of 0.2846 nm. That is, the LPG-OADM designed by this method can attain the ITU specification for the dense wavelength-division multiplexer (DWDM) bandwidth.

V. Conclusion

This study combined the FEM and the EEM with a rigorous, simplistic, and comprehensive design process to propose a visual, graphic, and simplistic numerical simulation method for designing and analyzing LPG-OADM. For LPG-OADM of approximately 1 cm in length, no current numerical simulation methods can perform 3-D component analysis and design. Section III thoroughly explained why the mode expansion method requires less memory and time to complete large-scale LPG-OADM analyses and designs. This study extracted single period objects from the LPG-OADM periodic object and recalculated the solutions, which is the essence of the EEM. This section showed the distinctiveness and unique features of this study. Furthermore, Section IV introduced one of the core techniques of this study. In addition, numerous rigorous graphical results based on the proposed design flow were shown in this section. The goal was to enable novice learners or application-level designers new to the field of LPG-OADM to use an easier graphical method when learning traditional mode-coupled theory, and to minimize the likelihood of encountering formulaic and abstract mathematical models directly. This study used actual examples to verify that, under the operating wavelength of $\lambda = 1550$ nm, the LPG-OADM designed by this method has an FWHM of 0.2846 nm and an insertion loss and homo-dyne crosstalk of nearly 0. That is, the LPG-OADM designed by this method can reach the ITU specification for the DWDM bandwidth. In addition, the power dissipation condition and mode orthogonal values were calculated and verified using examples to ensure that they conformed to the design process specifications. This study supplemented traditional mode-coupled theory with a rigorous, simplistic, and graphical numerical technique to reduce the complexity and difficulty of understanding LPG-OADM.

References

[1] Y. K. Chen, C. J. Hu, C. C. Lee, K. M. Feng, M. K. Lu, C. H. Chang, Y. K. Tu, and S. L. Tzeng, "Low-crosstalk and compact optical add-drop multiplexer using a multiport circulator and fiber Bragg grating," *IEEE Photon. Technol. Lett.*, vol. 12, no. 10, pp. 1394–1396, Oct. 2000.

[2] A. V. Tran, W. D. Zhong, R. C. Tucker, and R. Lauder, "Optical add-drop multiplexers with low crosstalk," *IEEE Photon. Technol. Lett.*, vol. 13, no. 6, pp. 582–584, Jun. 2001.

[3] F. Bilodeau, K. O. Hill, B. Malo, D. C. Johnson, and J. Albert, "High-return-loss narrowband all-fiber bandpass Bragg transmission filter," *IEEE Photon. Technol. Lett.*, vol. 6, no. 1, pp. 80–82, Jan. 1994.

[4] T. Erdogan, T. A. Strasser, M. A. Milbrodt, E. J. Laskowski, C. H. Henry, and G. E. Kohnke, "Integrated-optical Mach-Zehnder add-drop filter fabricated by a single UV-induced grating exposure," *Appl. Opt.*, vol. 36, pp. 7838–7845, 1997.

[5] C. Riziotis and M. N. Zervas, "Design considerations in optical add/drop multiplexers based on grating-assisted null couplers," *J. Lightw. Technol.*, vol. 19, pp. 92–104, 2001.

[6] K. S. Chiang, Y. Liu, N. Ng, and S. Li, "Coupling between two parallel long-period fiber gratings," *Electron. Lett.*, vol. 36, pp. 1408–1409, 2000.

[7] A. M. Vengsarkar, P. J. Lemaire, J. B. Judkins, V. Bhatia, T. Erdogan, and J. E. Sipe, "Long-period fiber gratings as band-rejection filters," *J. Lightw. Technol.*, vol. 14, pp. 58–65, 1996.

[8] A. M. Vengsarkar, J. R. Pedrazzani, J. B. Judkins, and P. J. Lemaire, "Long-period fiber-grating based gain equalizers," *Opt. Lett.*, vol. 21, pp. 336–338, 1996.

[9] D. Stegall and T. Erdogan, "Dispersion control with use of long-period fiber gratings," *J. Opt. Soc. Amer. A*, vol. 17, pp. 304–312, 2000.

[10] B. Judkins and A. M. Vengsarkar, "Optical fiber long-period grating sensors," *Opt. Lett.*, vol. 21, pp. 692–694, 1996.

[11] J. A. Besley, T. Wang, and L. Reekie, "Fiber cladding mode sensitivity characterization for long-period gratings," *J. Lightw. Technol.*, vol. 21, pp. 848–853, 2003.

[12] H. J. Patrick, A. D. Kersey, and F. Bucholtz, "Analysis of the response of long period fiber gratings to the external index of refraction," *J. Lightw. Technol.*, vol. 16, pp. 1606–1612, 1998.

[13] R. Falciai, A. G. Mignani, and A. Vannini, "Long period gratings as solution concentration sensors," *Sens. Actuators B*, vol. 74, pp. 74–77, 2001.

[14] Y. J. He, Y. L. Lo, and J. F. Huang, "Bandwidth analysis of long-period fiber grating for high order cladding mode and its application to optical add-drop multiplexer," *Opt. Eng.*, vol. 45, no. 12, pp. 125001-1–125001-8, 2006.

[15] W. H. Loh, F. Q. Zhou, and J. J. Pan, "Novel designs for sampled grating based multiplexers demultiplexers," *Opt. Lett.*, vol. 24, pp. 1457–1459, 1999.

[16] Y. J. He, Y. L. Lo, and J. F. Huang, "Optical-fiber surface-plasmon-resonance sensor employing long-period fiber grating in multiplexing," *J. Opt. Soc. Amer. B*, vol. 23, pp. 801–811, 2006.

[17] Ó. Esteban, R. Alonso, M. C. Navarrete, and A. González-Cano, "Surface plasmon excitation in fiber-optical sensors: A novel theoretical approach," *J. Lightw. Technol.*, vol. 20, pp. 448–453, 2002.

[18] T. Erdogan, "Cladding-mode resonances in short and long period fiber grating filters," *J. Opt. Soc. Amer. A*, vol. 14, pp. 1760–1773, 1997.

[19] T. Erdogan, "Fiber grating spectra," *J. Lightw. Technol.*, vol. 15, pp. 1277–1294, 1997.
[20] D. Sun, J. Manges, Y. Xingchao, and Z. Cendes, "Spurious modes in finite-element methods," *IEEE Antennas Propag. Mag.*, vol. 37, no. 5, pp. 12–24, Oct. 1995.
[21] C. H. Herry and Y. Shani, "Analysis of mode propagation in optical waveguide devices by Fourier expansion," *IEEE J. Quantum Electron.*, vol. 27, no. 3, pp. 523–530, Mar. 1991.
[22] G. Sztefka and H. P. Nolting, "Bidirectional eigenmode propagation for large refractive index steps," *IEEE Photon. Technol. Lett.*, vol. 5, no. 5, pp. 554–557, May 1993.
[23] D. F. G. Gallagher and T. P. Felici, "Eigenmode expansion methods for simulation of optical propagation in photonics: Pros and cons," *Proc. SPIE*, vol. 4987, pp. 69–82, 2003.

Yue Jing He received the M.S. degree from the Department of Communication Engineering, National Chiao-Tung University, Hsinchu, Taiwan, in 2000, and the Ph.D. degree from the Department of Electrical Engineering, National Cheng Kung University, Tainan, Taiwan, in 2006. After graduation, he has been a member of the faculty of the Department of Electronic Engineering, National Chin-Yi University of Technology, Taichung, Taiwan, since 2008. His research interests include the component design in optical fiber communication and in surface plasmon resonance sensor.

Xuan Yang Chen was born in Taoyuan, Taiwan, in March 1990. He received the B.E.E. degree from the Department of Electronic Engineering, National Chin-Yi University of Technology, Taichung, Taiwan, in 2012, where he is currently working toward the M.S. degree in the area of fiber-optic networking communications. His major interests include long period fiber grating device and surface plasmon sensors.